# Flow of anisometric particles in a quasi-two-dimensional hopper

Balázs Szabó,[1] Zsolt Kovács,[1] Sandra Wegner,[2] Ahmed Ashour,[2,3] David Fischer,[2] Ralf Stannarius,[2] and Tamás Börzsönyi[1,*]

[1]*Institute for Solid State Physics and Optics, Wigner Research Centre for Physics, Hungarian Academy of Sciences,*
*P. O. Box 49, H-1525 Budapest, Hungary*
[2]*Institute of Physics, Otto-von-Guericke-University, D-39106 Magdeburg, Germany*
[3]*Faculty of Engineering and Technology, Future University in Egypt, New Cairo, Egypt*

The stationary flow field in a quasi-two-dimensional hopper is investigated experimentally. The behavior of materials consisting of beads and elongated particles with different aspect ratio is compared. We show, that while the vertical velocity in the flowing region can be fitted with a Gaussian function for beads, in the case of elongated grains the flowing channel is narrower and is bordered with sharper velocity gradient. For this case, we quantify deviations from the Gaussian velocity profile. Relative velocity fluctuations are considerably larger and slower for elongated grains.

## I. INTRODUCTION

Hopper flows are very important in agriculture and various industrial processes dealing with granulates. The basic features of such flows have been characterized in numerous experimental and numerical studies for spherical grains, and more recently increasing attention has been payed to systems involving nonspherical particles. One of the fundamental questions relates to the outflow rate as a function of the orifice size, for which a power-law behavior was found by Beverloo *et al.* [1]. This relationship has been tested for various materials and was fine-tuned for the small particle-to-outlet diameter ratio limit [2]. Comparing the flow rate of spherical and slightly elongated particles (with equal volume) numerical discrete element method (DEM) studies predicted [3–5] that for frictional grains increasing particle elongation leads to lower flow rates, which was recently confirmed by experimental investigations [6]. On one hand, this might be counterintuitive, as elongated grains undergo shear induced orientational ordering with their average orientation pointing almost in the direction of the flow lines [7–11]. On the other hand, several authors have shown that for other nonspherical grains increasing grain angularity (or, in other words, increasing effective friction of the material) reduces the mass flow rate [3,4,12–15] and leads to larger stagnant zones and more residual mass after discharge [12,13,16,17]. Several authors detected and quantified fluctuations in the discharge rate or flow field [18–21]. The amplitude of the relative fluctuations of the discharge rate [21,22] or flow velocity [23] was shown to increase with decreasing orifice size and, finally, the probability for clogging [24,25] appears to increase with increasing particle aspect ratio (length $L$ to diameter $d$) [6].

The flow field inside a hopper can be approximated from microscopic arguments. In the void model of Litwiniszyn and Mullins [26,27] particles move downward by falling into holes below them, and thus the flow is related to directed (upward)

random walks of particle sized voids from the orifice. This leads to a Gaussian velocity profile across the hopper as it was elaborated in the kinematic model of Nedderman and Tüzün [28]. Even though the diffusive nature and the Gaussian profile was experimentally confirmed by several groups using beads [19,29,30], particle tracking or DEM simulations did not confirm the simple microscopic mechanism described above [31,32]. Namely, in the diffusion equation, the diffusion constant was shown to depend on the distance from the orifice [19,29,33]. Bazant and Rycroft showed that considering the collective rearrangement of a spot of grains ("*spot model*") better microscopic agreement is observed, and the introduction of a new length scale (spot size) helped to resolve some of the discrepancies [34,35]. This idea was further elaborated as a "stochastic flow rule" [36,37] or nonlinear elastoplastic model [38], capable of describing flowing regions and stagnant zones in granular flows simultaneously. Another recent numerical work by Staron *et al.* showed that the velocity profiles obtained by a discrete contact dynamics algorithm are reproduced when the $\mu(I)$ flow law (obtained experimentally for glass beads [39,40]) is incorporated into a continuum Navier-Stokes solver [41].

The flow field for nonspherical grains is less investigated. Pioneering particle image velocimetry (PIV) measurements were carried out with cylinders of aspect ratio close to 1 and slightly nonspherical (amaranth) grains [42,43], but the given sample velocity profiles were not fitted by any function. Ellipses with an aspect ratio of 1.3 were also tested in a two-dimensional (2D) silo [44]. Although the experimental data were quite noisy, they were fitted using a Gaussian function. More recently, the velocity profile for Amaranth grains was found to be closer to a parabolic function than to a Gaussian [45]. Discrete element simulations with corn shaped particles reported slightly larger grain velocity in the center of the hopper compared to the case of beads, but no further analysis of the velocity profiles was presented [46,47].

In the present work we determine the velocity fields by PIV analysis for glass rods with two different aspect ratios ($L/d =$ 1.4 and $L/d = 3.5$), plastic rods with $L/d = 6$, lentils (aspect
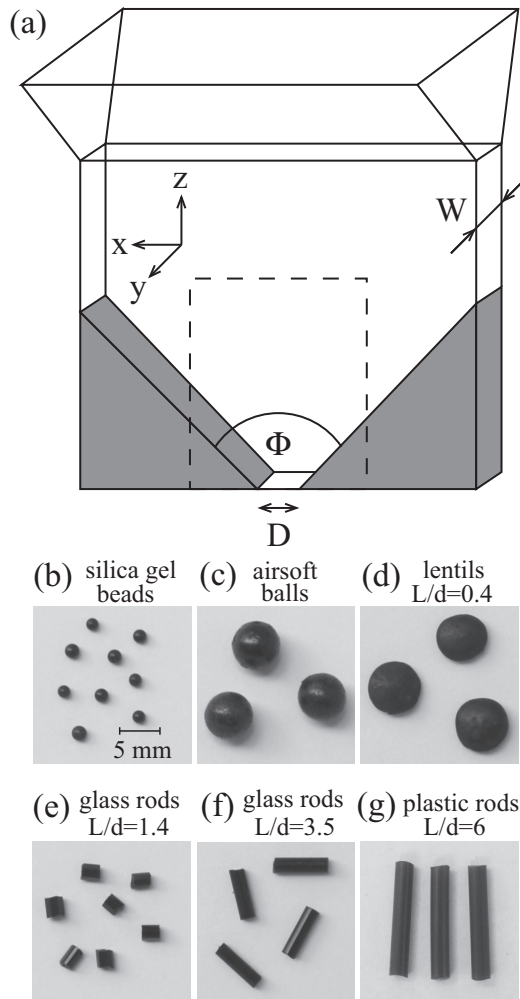
*borzsonyi.tamas@wigner.mta.hu

FIG. 1. (a) Schematic view of the experimental geometry. Dashed line indicates the observation area. [(b)–(g)] Photographs of the granular samples.

ratio of 0.4), and two type of beads (silica gel and plastic). We observe and quantify deviations from the Gaussian velocity profile for rods. We show that the amplitude of temporal fluctuations of the velocity field systematically increases with particle elongation.

## II. EXPERIMENTAL METHODS

In our experiments a quasi-two-dimensional hopper was used [see Fig. 1(a)], with horizontal and vertical dimensions of 700 and 600 mm, respectively. The central area (290 mm × 370 mm) was recorded by a digital camera (MotionBLITZ EoSens mini, 1.3 MPixel with a frame rate of 200 fps). The distance between the two glass plates $W$ was set to 18 mm (similar results were obtained with $W = 35$ mm). The additional reservoir at the top of the hopper helped reducing finite-size effects, i.e. ensured that the flow field is not influenced by surface distortions of the quasi-two-dimensional granular layer. In the measurements presented here we used four different orifice sizes $D$ (15–45 mm) and seven different values (46°–140°) of the inclination angle $\Phi$ of the wedge-shaped walls. The flow field, which is essentially restricted to a two-dimensional

plane, was detected by a self-written PIV algorithm, which is basically similar to other freely or commercially available PIV codes. Focusing on vertical motion, the box size for correlating segments of the subsequent images was chosen to be much larger in the $z$ direction than the $x$ direction. This allowed us to determine the vertical displacement of the image segments with high (subpixel) resolution, low noise, and with increased horizontal resolution of the data points. This algorithm was used to determine high-frequency oscillations in a cylindrical hopper flow [48] or high-resolution displacement profiles in sheared granular media [49]. In the present study, three measurements were recorded for each setting, and the results were averaged to reduce statistical fluctuations. Photographs of the six granular samples are shown in Fig. 1: spherical silica gel beads [$d = 1.8$ mm, Fig. 1(b)], airsoft balls [$d = 6.0$ mm, Fig. 1(c)], and oblate lentil seeds [$L = 2.5$ mm, $d = 6.4$ mm, $L/d = 0.4$, Fig. 1(d)] and short glass rods [$L = 2.5$ mm, $d = 1.8$ mm, $L/d = 1.4$, Fig. 1(e)], long glass rods [$L = 6.6$ mm, $d = 1.9$ mm, $L/d = 3.5$, Fig. 1(f)], and plastic rods [$L = 14$ mm, $d = 2.33$ mm, $L/d = 6.0$, Fig. 1(g)]. The choice of materials allows us to investigate new types of beads (silica gel and plastic) to complement earlier measurements on glass beads [19,29] and steel beads [30] and to study the case of nonspherical particles with similar size as the beads.

In the experimental procedure the cell was filled first by closing the outlet and pouring the granulates from above. When the flow was started, an initial transient occurred, during which
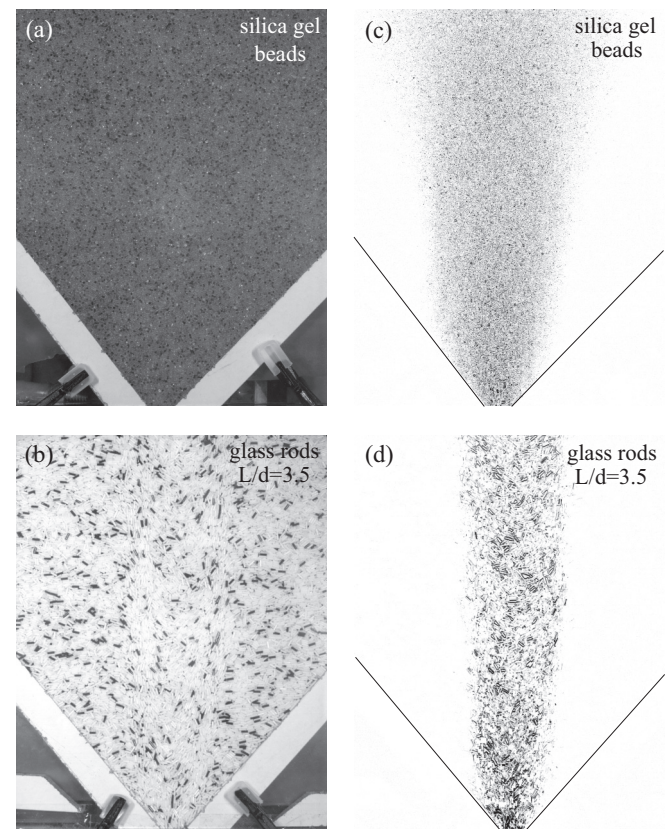


FIG. 2. (a) Sample images of the flow for (a) silica gel beads and (b) glass rods with $L/d = 3.5$. [(c) and (d)] The flowing region visualized by image differencing.

the width of the flow was continuously decreasing. After a few seconds, the flow profile became stationary. Near the end of the run, the free surface of the granular layer approached the observation area, and the flow profile became wider again. We focus on the stationary flow between the initial and final transients.

Sample images taken during stationary flow are presented for silica gel beads and for glass rods with $L/d = 3.5$ in Figs. 2(a) and 2(b). Visualizing the moving regions [Figs. 2(c) and 2(d)] by taking the difference of subsequent images shows that flow is concentrated in a narrower channel (i.e., the stagnant zone is larger) for the case of rods. A video showing the temporal evolution of the system can be found in the Supplemental Material [50], where a third column is inserted showing the velocity field calculated by the PIV algorithm.

## III. RESULTS

In order to quantitatively compare the flow fields for different materials, the time-averaged vertical velocity $[v_z(x)]$ has been determined across the sample. These profiles are shown in Fig. 3(a) at the height of $z = 60\, d^*$ for all six samples at the same dimensionless orifice size $D \approx 7.5\, d^*$. Here $d^*$ stands for the equivalent diameter of a sphere having the same volume as the elongated particle.

The velocity curves have been fitted with the function:

$$v_z = c \exp\left[-\left(\frac{2|x|}{x_0}\right)^\eta\right], \tag{1}$$

where the exponent $\eta$ quantifies deviations from the Gaussian ($\eta = 2$) velocity profile, and $x_0$ is the half width of the flowing channel. Larger $\eta$ make the slopes of the profile steeper and small $\eta < 2$ smoothens the profile. These two parameters have been determined as a function of the vertical coordinate $z$ and are shown in Figs. 3(b) and 3(c). As seen, for three samples the exponent $\eta$ stays around 2 and the normalized value of the channel width ($x_0/d^*$) is increasing with $z$ very similarly. As mentioned above, the velocity profiles were shown to be Gaussian for spherical glass beads [19,29] and steel beads [30] in earlier studies. Our data for beads nicely confirm the appropriateness of Gaussian fits for two further types of material: silica gel and plastic airsoft balls. The case of smooth oblate particles (lentils) also appear to obey this rule. For the three samples consisting of rods, however, the exponent $\eta$ becomes significantly larger than 2 above a certain value of $z$. At around the same height the flow width $x_0/d^*$ starts deviating from the other three curves. Thus for the case of rods above a certain height, the velocity profile is characterized by a plateau with relatively narrow shear zones at the two sides. The height above which the exponent $\eta$ substantially deviates from 2 depends on the grain shape and is about 20 $d^*$ for rods with $L/d = 3.5$ and $L/d = 6$ and around 100 $d^*$ for rods with $L/d = 1.4$. This shows, that the velocity field for the longer rods ($L/d = 3.5$ and $L/d = 6$) is non-Gaussian almost in the entire hopper, while for $L/d = 1.4$ a region right above the outlet remains Gaussian. We note that the largest value of
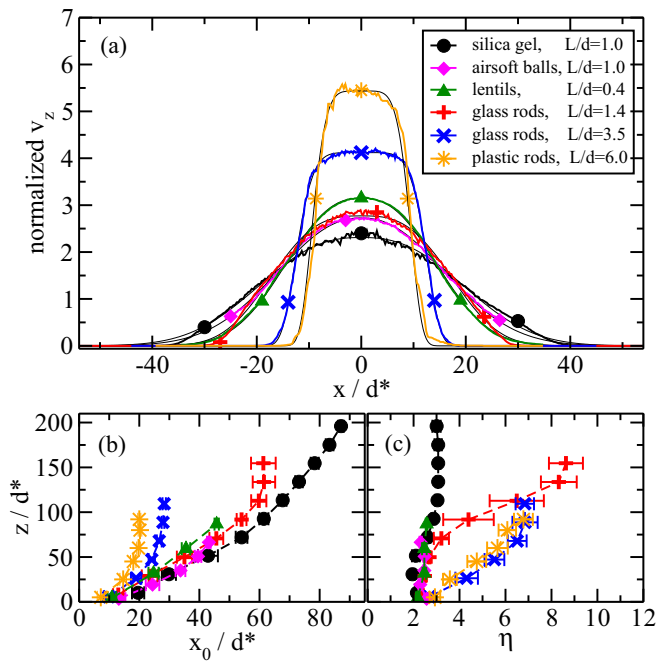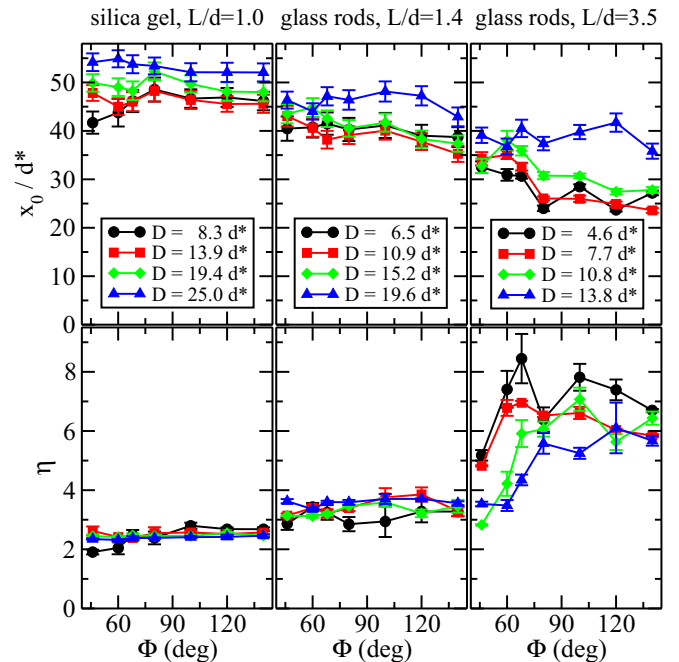
FIG. 3. (a) Time-averaged vertical velocity as a function of $x$, at height $z = 60\, d^*$, for all six materials. The curves are normalized by the integral of the fitted functions [Eq. (1)], symbols are displayed on each curve for a better distinction. The thin black lines represent the fitted curves. [(b) and (c)] The two fitting parameters: the exponent $\eta$ and the half width of the flowing channel $x_0$ [defined in Eq. (1)] at different heights. Both $x_0$ and the height coordinate $z$ are in units of the effective particle diameter $d^*$. For each material the outlet size was $D \approx 7.5\, d^*$ and the angle of the wedge shaped walls was set to $\Phi = 80°$.

FIG. 4. The two parameters describing the velocity profile: The exponent $\eta$ and the normalized half width $x_0/d^*$ [see Eq. (1)] as a function of the hopper angle $\Phi$, at a height of $z = 60\, d^*$, for three of the investigated materials. The lines are a guide to the eye.

the exponent $\eta$ is detected for these shorter rods ($L/d = 1.4$), and we will get back to this observation later.

The systematic change in the exponent $\eta$ and the half width of the flowing channel $x_0$ by changing the grain elongation is also demonstrated in Fig. 4. We see that this behavior appears to be general, as both $\eta$ and $x_0$ do not change significantly when changing the hopper angle $\Phi$ or the orifice size $D$. Looking at the details, a slight increase of $x_0$ can be noted with increasing $D$ for all three materials and with decreasing $\Phi$ for rods. In the experiments with longer glass rods, deviations from the Gaussian profile are stronger (i.e., $\eta$ is larger) for larger hopper angles $\Phi$.

The movie presented in the Supplemental Material [50] visualizes temporal fluctuations of the flow velocity. The time evolution of the velocity taken in the central part of the hopper at $z = 60\,d^*$ is shown in Fig. 5(a). As it is seen, the amplitude of relative deviations from the mean velocity systematically increases with grain elongation. This is quantified by the standard deviation $\sigma$ of the normalized velocity data which is shown as a function of $L/d$ in the inset of Fig. 5(b). We note that the actual time sequences are longer (about 4 s), Fig. 5(a) shows only a 1-s interval, so that the timescale of the fluctuations is better seen. Another way to characterize the time sequences is to measure the asymmetry of the fluctuations. This can be quantified by the fraction of velocity data points above and below the average, which are distributed at 53:47 for silica gel, 56:44 for short glass rods, 42:58 for long glass rods, and 41:59 for plastic rods with $L/d = 6$. The asymmetry is increasing with grain elongation, and notably it changes sign for the samples with longer grains which show larger velocity
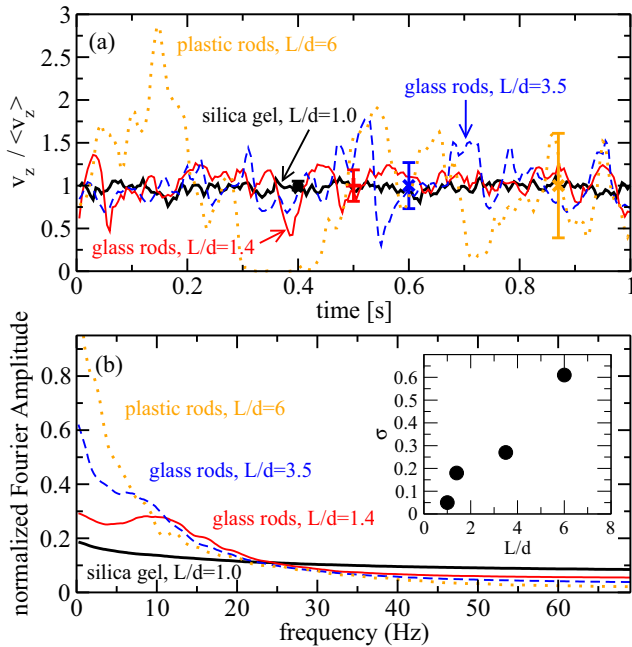
fluctuations. As described above, three independent runs were performed for each material. The mean velocity calculated for these runs varied less than 1.5% for silica gel, 3% for rods with $L/d = 1.4$, 12% for rods with $L/d = 3.5$, and 10% for rods with $L/d = 6$. Thus even if the velocity fluctuations were relatively large, the mean velocity measured in independent runs varied comparably little.

Performing a Fourier analysis of the $v_z(t)$ signals reveals that increasing grain elongation leads to increasing amplitude in the low-frequency range of the power spectrum [see Fig. 5(b)]. For rods with $L/d = 1.4$ and $L/d = 3.5$, noticeable peaks are seen at around $\approx 10$ Hz and $\approx 7$ Hz, respectively. Thus, for longer grains the velocity field fluctuates with larger amplitude and lower frequency. From this respect, it would be worth investigating fully 3D hoppers, where the orientation of rods is not influenced by the confining walls. In any case, the above described observation is coherent with our recent findings on 3D hoppers, where an increasing aspect ratio of the grains lead to lower flow rates and higher clogging probabilities compared to spherical grains [6].

In the following, we analyze the effect of the fluctuations on the shape of the velocity profile. Figure 6 presents velocity
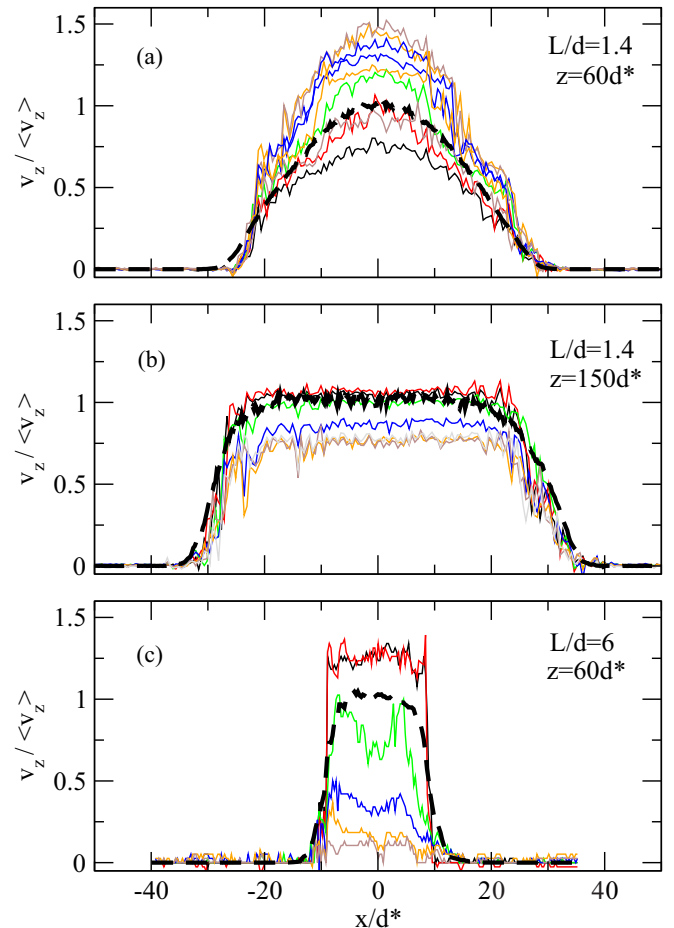
FIG. 5. (a) Temporal fluctuations in the velocity values above the orifice at $z = 60\,d^*$. (b) Fourier power spectrum of the curves presented in panel (a), normalized by their integral across the whole frequency range (from 0 to 70 Hz). The inset shows the standard deviation of the velocity data as a function of the particle elongation $L/d$.

FIG. 6. The form of velocity profiles during fluctuations for rods with $L/d = 1.4$ at (a) $z = 60\,d^*$ and (b) $z = 150\,d^*$ and (c) rods with $L/d = 6$ at $z = 60\,d^*$. Different colors represent different instant velocity profiles, the dashed lines show the time-averaged velocity profile for the whole run.

profiles taken from subsequent frames of the image sequence from a selected period of time, when the velocity changes significantly. Figures 6(a) and 6(b) show the case of rods with $L/d = 1.4$ at the elevations of $z = 60\,d^*$ and $z = 150\,d^*$. As it is seen, the shape of the velocity profile remains similar, even if the velocity value changes substantially. The time-averaged velocity profile (shown with a dashed line) is very similar to the instantaneous profiles. We see a Gaussian-like profile in the lower part of the hopper and a profile with a clear plateau and narrow shear zones at the two sides at a higher elevation. The shape difference is clearly captured by the exponent $\eta$ [see Fig. 3(c)] which is between 2 and 3 for $z = 60\,d^*$ and around 9 for $z = 150\,d^*$.

Turning to the case of rods with $L/d = 6$ we see that velocity fluctuations are so large that they are already affecting the shape of the velocity profile. Figure 6(c) shows one of the most violent events, where the velocity profile collapses and the flow almost stops. We see that the velocity profile before collapse has a clear plateau and sharp steps (very narrow shear zones) at the two sides. During collapse, however, its shape changes significantly. Such shape changes lead to the fact that the steps on the two sides of the time-averaged velocity profile [shown with a dashed line in Fig. 6(c)] became less steep, resulting in a smaller value of the exponent $\eta$ (about 5.6 in this case) than for rods with $L/d = 1.4$. This effect was clearly noticeable for rods with $L/d = 3.5$ and $L/d = 6$. In a way, this strange behavior of long grains is in qualitative agreement with observations of long cylindrical particles in 3D silos. There we have identified "rat holes" which form above the orifice when the aspect ratio of the particles becomes larger than 6 [6]. Those holes represent vertical tunnels with stable side walls above the orifice, where the material remains stagnant at the sides of the rat hole, while the silo empties only by the material inside

the rat hole. The silo discharge stops even without clogging when the rat hole penetrates the granular bed in the silo and reaches the surface. In the 2D experiments, we see essentially the same feature that the material remains stagnant at the sides and flow is restricted to a kind of two-dimensional rat hole above the orifice. The outflow does not come to a complete rest, and violent avalanches can destroy part of the stagnant zones temporarily.

## IV. SUMMARY

We have experimentally studied the flow field of a granular material in a quasi-two-dimensional hopper. Using six granular samples with different grain shapes (spherical, oblate, and prolate), we find that the velocity profile—characterizing the downward motion of the grains—can be well fitted with a Gaussian function for spherical particles as earlier models predicted; however, for elongated grains the flow field has a different form. In that case the flowing region is narrower and is bordered with sharper velocity gradient. We quantified the deviation of the velocity profile from the Gaussian form by measuring the exponent $\eta$ as a function of the vertical position in the hopper. Focusing on the time evolution of the velocity profile, we find that the flow of elongated grains is characterized by velocity fluctuations of larger amplitude and lower frequency compared to the case of spheres.

## ACKNOWLEDGMENTS

[1] W. A. Beverloo, H. A. Leniger, and J. van de Velde, Chem. Eng. Sci. **15**, 260 (1961).

[2] C. Mankoc, A. Janda, R. Arévalo, J. M. Pastor, I. Zuriguel, A. Garcimartín, and D. Maza, Granular Matter **9**, 407 (2007).

[3] P. W. Cleary, *Second International Conference on CFD in the Minerals and Process Industries* (CSIRO, Melbourne, Australia, 1999), pp. 71–76.

[4] P. W. Cleary and M. L. Sawley, Appl. Math. Modelling **26**, 89 (2002).

[5] S. D. Liu, Z. Y. Zhou, R. P. Zou, D. Pinson, and A. B. Yu, Powder Technol. **253**, 70 (2014).

[6] A. Ashour, S. Wegner, T. Trittel, T. Börzsönyi, and R. Stannarius, Soft Matter **13**, 402 (2017).

[7] G. W. Baxter and R. P. Behringer, Phys. Rev. A **42**, 1017 (1990).

[8] K. A. Reddy, V. Kumaran, and J. Talbot, Phys. Rev. E **80**, 031304 (2009).

[9] C. S. Campbell, Phys. Fluids **23**, 013306 (2011).

[10] T. Börzsönyi, E. Somfai, B. Szabó, S. Wegner, P. Mier, G. Rose, and R. Stannarius, New J. Phys. **18**, 093017 (2016).

[11] T. Börzsönyi, B. Szabó, G. Törös, S. Wegner, J. Török, E. Somfai, T. Bien, and R. Stannarius, Phys. Rev. Lett. **108**, 228302 (2012).

[12] D. Höhner, S. Wirtz, and V. Scherer, Powder Technol. **226**, 16 (2012).

[13] D. Höhner, S. Wirtz, and V. Scherer, Powder Technol. **235**, 614 (2013).

[14] B. Sukumaran and A. K. Ashmawy, Powder Technol. **138**, 46 (2003).

[15] B. Soltanbeigi, A. Podlozhnyuk, J. Y. Ooi, C. Kloss, and S. A. Papanicolopulos, EPJ Web Conf. **140**, 06015 (2017).

[16] A. Gupta, S. Nag, and Tathavadkar, Int. J. Miner. Process. **110-111**, 135 (2012).

[17] J. Wu, J. Chen, and Y. Yang, Powder Technol. **181**, 74 (2008).

[18] G. W. Baxter, R. P. Behringer, T. Fagert, and G. A. Johnson, Phys. Rev. Lett. **62**, 2825 (1989).

[19] A. Medina, J. A. Cordova, E. Luna, and C. Trevino, Phys. Lett. A **250**, 111 (1998).

[20] G. Mollon and J. Zhao, Granular Matter **15**, 827 (2013).

[21] R. O. Uñac, A. M. Vidales, O. A. Benegas, and I. Ippolito, Powder Technol. **225**, 214 (2012)

[22] A. Janda, R. Harich, I. Zuriguel, D. Maza, P. Cixous, and A. Garcimartín, Phys. Rev. E **79**, 031302 (2009).

[23] C. C. Thomas and D. J. Durian, Phys. Rev. E **94**, 022901 (2016).

[24] I. Zuriguel, A. Garcimartín, D. Maza, L. A. Pugnaloni, and J. M. Pastor, Phys. Rev. E **71**, 051303 (2005).

[25] I. Zuriguel, D. R. Parisi, R. C. Hidalgo, C. Lozano, A. Janda, P. A. Gago, J. P. Peralta, L. M. Ferrer, L. A. Pugnaloni, E. Clément, D. Maza, I. Pagonabarraga, and A. Garcimartín, Sci. Rep. **4**, 7324 (2014).

[26] J. Litwiniszyn, Bull. Acad. Pol. Sci., Ser. Sci. Technol. **11**, 61 (1963).

[27] W. W. Mullins, J. Appl. Phys. **43**, 665 (1972).

[28] R. M. Nedderman and U. Tüzün, Powder Technol. **22**, 243 (1979).

[29] J. Choi, A. Kudrolli, and M. Z. Bazant, J. Phys.: Condens. Matter **17**, S2533 (2005).

[30] A. Garcimartín, I. Zuriguel, A. Janda, and D. Maza, Phys. Rev. E **84**, 031309 (2011).

[31] R. Arévalo, A. Garcimartín, and D. Maza, Eur. Phys. J. E **23**, 191 (2007).

[32] J. Choi, A. Kudrolli, R. R. Rosales, and M. Z. Bazant, Phys. Rev. Lett. **92**, 174301 (2004).

[33] R. Balevičius, R. Kačianauskas, Z. Mróz, and I. Sielamowicz, Adv. Powder Technol. **22**, 226 (2011).

[34] M. Z. Bazant, Mech. Mater. **38**, 717 (2006).

[35] C. H. Rycroft, M. Z. Bazant, G. S. Grest, and J. W. Landry, Phys. Rev. E **73**, 051306 (2006).

[36] K. Kamrin and M. Z. Bazant, Phys. Rev. E **75**, 041301 (2007).

[37] K. Kamrin, C. H. Rycroft, and M. Z. Bazant, Modell. Simul. Mater. Sci. Eng. **15**, S449 (2007).

[38] K. Kamrin, Int. J. Plast. **26**, 167 (2010).

[39] P. Jop, Y. Forterre, and O. Pouliquen, J. Fluid Mech. **541**, 167 (2005).

[40] P. Jop, Y. Forterre, and O. Pouliquen, Nature **441**, 727 (2006),

[41] L. Staron, P.-Y. Lagrée, and S. Popinet, Eur. Phys. J. E **37**, 5 (2014).

[42] D. A. Steingart and J. W. Evans, Chem. Eng. Sci. **60**, 1043 (2005).

[43] I. Sielamowicz, S. Blonski, and T. A. Kowalewski, Chem. Eng. Sci. **60**, 589 (2005).

[44] J. F. Favier, M. H. Abbaspour-Fard, and M. Kremmer, J. Eng. Mech. **127**, 971 (2001).

[45] I. Sielamowicz, M. Czech, and T. A. Kowalewski, Biosystems Eng. **108**, 334 (2011).

[46] H. Tao, B. Jin, W. Zhong, X. Wang, B. Ren, Y. Zhang, and R. Xao, Chem. Eng. Proc. **49**, 151 (2010).

[47] C. González-Montellano, E. Gallego, Á. Ramírez-Gómez, and F. Ayuga, Comput. Chem. Eng. **40**, 22 (2012).

[48] T. Börzsönyi and Z. Kovács, Phys. Rev. E **83**, 032301 (2011)

[49] B. Szabó, J. Török, E. Somfai, S. Wegner, R. Stannarius, A. Böse, G. Rose, F. Angenstein, and T. Börzsönyi, Phys. Rev. E **90**, 032205 (2014)

[50] See Supplemental Material at http://link.aps.org/supplemental/10.1103/PhysRevE.97.062904 for a short video demonstrating the differences in the flow field for different particle shapes.